Non-Ohmic effects in hopping conduction in doped silicon and germanium between 0.05 and 1 K

J. Zhang,* W. Cui,[†] M. Juda,* and D. McCammon
Department of Physics, University of Wisconsin, Madison, Wisconsin 53706

R. L. Kelley, S. H. Moseley, C. K. Stahle, and A. E. Szymkowiak
NASA/Goddard Space Flight Center, Greenbelt, Maryland 20771

We have studied non-Ohmic effects in hopping conduction in moderately compensated ion-implanted Si:P, B (both n- and p-type) and neutron-transmutation-doped Ge:Ga,As over the temperature range 0.05–0.8 K and up to moderately strong electric fields. In the limit of small fields, where the current is proportional to applied voltage, the resistivities of these materials are approximated over a wide temperature range by the model of variable range hopping with a Coulomb gap: $\rho = \rho_0 \exp(T_0/T)^{1/2}$. The samples included in this study have characteristic temperatures T_0 in the range 1.4–60 K for silicon, and 22–60 K for germanium. We have compared our data to exponential and "hyperbolic-sine" field-effect models of the electrical nonlinearity: $\rho(E) = \rho(0)e^{-x}$ and $\rho(E) = \rho(0)x/\sinh(x)$, where $x \equiv eEl/kT$, and to an empirical hot-electron model. The exponential field-effect model tends to be a good representation for the samples with high T_0 at low T. The sinh model can match the data only at low fields. The hot-electron model fits our data well over a wide range of power in the low-T_0–high-T regime. We discuss the quantitative implications of these results for the application of these materials as thermometers for microcalorimeters optimized for high-resolution spectroscopy. [S0163-1829(98)05208-4]

I. INTRODUCTION

We have conducted a series of experiments to study the non-Ohmic behavior of doped silicon and germanium as part of a program to characterize heavily doped semiconductors operating in the hopping conduction regime for use as thermometers in single-photon x-ray calorimeters. These calorimeters offer much higher energy resolution for soft x rays than conventional solid-state detectors.

The theory of operation of calorimeters with ideal resistive thermometers has been discussed by Moseley, Mather, and McCammon.[1] Taking into account only thermodynamic fluctuations and thermometer Johnson noise, the energy resolution of a calorimeter is

$$\Delta E = \xi \sqrt{k T_s^2 C(T_s)}, \tag{1}$$

where k is Boltzmann's constant, T_s is the heat-sink temperature, $C(T_s)$ is the total heat capacity of the detector at T_s and ξ is a numerical factor that is a decreasing function of the temperature sensitivity of the thermistor. Therefore, achieving high-energy resolution requires low operating temperature, low total heat capacity, a sensitive thermometer, and minimization of any additional noise sources.

A good thermometer for a calorimeter has high-temperature sensitivity, a good match to a low-noise readout, low heat capacity, and convenient construction. Doped silicon thermistors offer several advantages as thermometers for x-ray calorimeters. There is a considerable body of experience in their use in infrared bolometers,[2,3] and well-developed integrated circuit processing techniques for silicon allow one to control the thermistor volume to minimize its contribution to the total heat capacity, and to integrate the thermistor into the detector structure without use of high specific-heat bonding materials.[4] It is also easy to construct the thermistor with the $\sim 10^7 \ \Omega$ impedance required to match an inexpensive silicon junction field-effect transistor operated at ~ 130 K. This provides a simple amplifier with a noise temperature below 10 mK at low audio frequencies.

The temperature dependence of the electrical resistance of our ion-implanted silicon samples in the Ohmic region can be approximated by

$$\rho = \rho_0 \exp(T_0/T)^{1/2}, \tag{2}$$

over a wide range in temperature as reported in Zhang *et al.*[5] (hereafter paper I). The resistivity shows a large electric-field dependence, or non-Ohmic behavior, when the field strength E or power per unit volume P/V is sufficiently large. Note that $E = \sqrt{\rho P/V}$, so there is no model-independent way to distinguish an electric-field effect from a power-density effect by scaling the dimensions of the device. Figure 1 shows an example of this behavior. It can be seen that non-Ohmic effects act to reduce the thermometer sensitivity: at sufficiently high electric fields the resistance becomes entirely independent of temperature.

Equation (1) shows that the total heat capacity should be minimized to make a calorimeter with the best possible energy resolution. Since doped silicon and germanium have much higher specific heats than the pure materials, this requires making the thermistor as small as possible. However, for a given calorimeter there is an optimum bias power level that gives the best signal-to-noise ratio.[1] At this bias power level, a small thermistor volume that minimizes total heat capacity gives a large P/V that results in serious non-Ohmic effects, reducing the temperature sensitivity. In addition, the volume reduction also increases an excess low-frequency noise that seems to be an intrinsic characteristic of this type
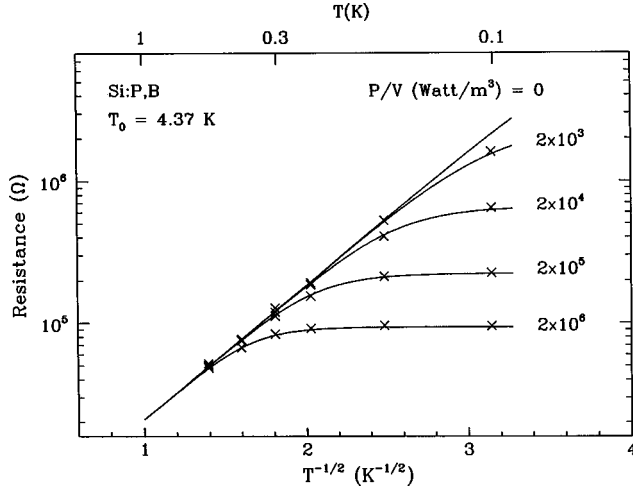
FIG. 1. Reduction in thermometer sensitivity at finite readout power densities. The solid lines are from the model discussed in Sec. V. (The data points are sparse because data are actually taken at constant temperature rather than constant power densities. All the data for this device are shown on the constant temperature plots in Fig. 5.)

of thermistor.[6] The non-Ohmic effects and excess noise make the thermistor a limitation on the energy resolution of these calorimeters. An understanding of the behavior of the non-Ohmic effects and excess noise is therefore necessary to optimize the detector design. We do not yet have sufficient data to quantify the behavior of the excess noise; in this paper we report the results from our study of the non-Ohmic effects.

As discussed below, both theoretical and experimental understandings of the non-Ohmic effects in hopping conduction are far from complete, and we did not find any adequate description of non-Ohmic effects in the range of temperature, power, and T_0 in which we are interested. We therefore made a series of measurements to gain sufficient empirical understanding of thermistor behavior to be able to optimize the design of detectors. We compare our data with an exponential field-effect model, a hyperbolic-sine field-effect model, and an empirical hot-electron model and find fairly systematic behavior that cannot easily be related to existing theories. Using empirical fits to the non-Ohmic behavior, we then discuss its effect on the temperature sensitivity of the thermistors.

II. MODELS

A. Field-effect models

The non-Ohmic effect in hopping conduction in doped semiconductors has received considerable theoretical study.[7-10] These models assume that field-assisted tunneling dominates the non-Ohmic behavior. There are several different analytic predictions for this effect. Hill considered the motion of charge carriers both along and against the electric field and obtained a dependence for the current density j on the electrical field E:[7]

$$j(T,E) \propto \sigma(T,0)E \sinh\left(C\frac{eE\lambda}{kT}\right), \qquad (3)$$

where e is electron charge, E is electric field, C is a constant on the order of unity, and λ is a characteristic hopping length. At sufficiently high fields, where $eE\lambda > kT$, the reverse current can be ignored. For this case, Hill derived

$$j(T,E) \propto \sigma(T,0)E \exp\left(C\frac{eE\lambda}{kT}\right). \qquad (4)$$

In the derivation of Eqs. (3) and (4), only the case that the Ohmic behavior follows the Mott law, $\rho = \rho_0 \exp(T_0/T)^{1/4}$, was considered, but the same field dependence can be obtained if the Ohmic behavior follows the Coulomb gap model [Eq. (2)]. Pollak and Reiss also derived Eq. (4) using a percolation method.[8]

Most of the published non-Ohmic data have been compared to Eq. (4) in the following form:

$$\rho(T,E) = \rho(T,0)\exp-\left(C\frac{eE\lambda}{kT}\right). \qquad (5)$$

This equation is different from Eq. (4) only by a factor of E, and such nonexponential dependence can be ignored in the spirit of this derivation.[7] The exponential field dependence fits a portion of the published experimental results to some extent.[11-18] We will say more about existing data in the discussion section. While other analytic predictions for the non-Ohmic behavior exist,[9,10] they do not provide a good fit to any published data nor to the data we present here. Some of the published data are not readily explained by any field-effect model.[19,20]

B. Hot-electron model

Hot-electron effects are expected at low temperatures in metals.[21-25] The standard model assumes that the applied I^2R power is deposited in the electron system, and that the energy that electrons pick up from the electric field is transferred to the heat sink only through electron-phonon interactions. At low temperatures, the electron-phonon coupling becomes so weak that the energy is distributed among electrons more rapidly than it can be transferred to the lattice. This leads to an electron energy distribution characterized by an electron temperature that is higher than the lattice temperature. Little[21] and Shklovskij[22] calculated the effective thermal conductance, $G_{e\text{-ph}}$, between the conducting electrons and the phonon system in a metal and found that $G_{e\text{-ph}} \propto T^4$.

In a metal, the electrons are free to move and the energy is distributed among the electrons via collisions, whereas in a doped semiconductor hopping conduction is the dominant conduction mechanism, and the electrons are localized. The physical justification for a hot-electron model is not so obvious in this case, and we know of no quantitative theoretical model (but see Ref. 26).

We can, however, use the hot-electron model as an alternative way to parametrize our data without worrying about its physical validity. We make three assumptions. First, the bias (I^2R) power is initially deposited entirely in the electron system. Second, the resistance of the thermistor depends only on the "electron temperature", T_e. The functional

form of $R(T_e)$ is not important, as it can be determined empirically from measurements at low power. In this study we used

$$R = R_0 \exp(T_0/T_e)^{1/2}, \qquad (6)$$

where R_0 and T_0 are derived from the low-field data, and are allowed to vary with temperature if necessary. Finally, the conductance per unit volume for energy transfer between the electron system and the phonon system is assumed to have a power-law dependence on T_e:

$$g_{e\text{-ph}} \equiv d(P/V)/dT_e = g_0 T_e^\beta, \qquad (7)$$

where P/V is the power per unit volume transferred between two systems. For a given power dissipation the electron temperature is then given by

$$T_e^{\beta+1} = \frac{\beta+1}{g_0} \frac{P}{V} + T_l^{\beta+1}, \qquad (8)$$

where T_l is the lattice temperature. Equations (6) and (8) can be used to predict the resistance for any given power dissipation, thermistor size, and lattice temperature. Good fits to this model have been published for doped Ge thermometers operated at very low temperatures.[19,20]

III. SAMPLE PREPARATION AND MEASUREMENT

Details of the preparation and characteristics of our ion-implanted silicon samples and of the measurement methods have been given in paper I (note that Table II of paper I had incorrect data for the n-type contact implants—a corrected version is published as an Erratum).[5] The ion-implanted Si:P,B samples used here have net doping densities in the range $2-5 \times 10^{18}$ cm^{-3} with 50% compensation. The implanted regions have thicknesses of about 0.2 μm and the lengths and widths range from 40 to 400 μm with a variety of aspect ratios. The neutron-transmutation-doped (NTD) Ge samples have a cross section of about 100×100 μm^2 and lengths of ~ 100 or ~ 400 μm. Sample preparation for NTD Ge has been described in Ref. 27.

In order to study non-Ohmic effects, it is important to verify that the resistance drop is not due to heating of the sample relative to the thermometers monitoring the heat sink temperature. For some of the doped silicon samples, we checked whether this was a significant effect by collecting data from one thermistor while using an electrically independent thermistor on the same die to monitor the lattice temperature. Since we did not make this check on all measurements, however, caution is necessary when considering data taken at the highest power levels.

For the NTD Ge samples, we did not monitor the lattice temperatures during the data collection, and the thermal contact area between the Ge samples and the TO-5 transistor headers was considerably smaller relative to the thermistor volume than for the silicon samples. Therefore, the lattice heating problem was more serious for the Ge samples. At high power dissipation levels in some Ge samples, we observed a decrease in resistance that is consistent with the T^3 temperature dependence expected from a finite interface thermal resistance between the Ge chip and its mount. We measured the thermal contact resistance for a Si sample, and
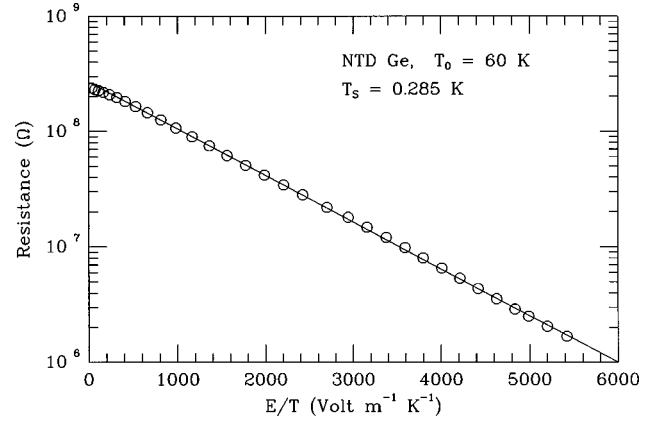

FIG. 2. An exponential field-effect model fit [Eq. (5)]. The data are from a NTD germanium sample at $T = 0.285$ K. The value of λ for the fit is 805 Å.

found that it was about the same per unit area as the apparent thermal resistance of the Ge samples. Using this assumption, we have excluded Ge data with potential lattice heating.

IV. EXPERIMENTAL RESULTS

In this section, we compare the non-Ohmic models discussed above to our data. The exponential field effect model of Eq. (5) provides a good fit to some but not all of the data. Figure 2 shows the best example of a good fit to this model. The data were taken from a NTD Ge sample at 0.285 K; this sample has $T_0 \sim 63$ K, where T_0 is from the fit of Eq. (2) to the low-field data.

For the cases where this model fits well, we investigated the temperature dependence of the parameter λ, the characteristic hopping length. Hill discussed this for the Mott-law case;[7] we have applied his method to the case where there is a Coulomb gap, and derive the following temperature dependence:

$$\lambda(T) = \frac{a}{2} \sqrt{T_0/T}, \qquad (9)$$

where a is the localization radius and T is the lattice temperature. The combination of Eqs. (5) and (9) gives

$$R(T,E) = R(T,0) \exp\left\{ \frac{e}{k} \frac{Ca\sqrt{T_0}}{2} \frac{E}{T^{3/2}} \right\}, \qquad (10)$$

where C is a constant of the order unity. According to Eq. (10), plotting the data as $\ln R$ versus $E/T^{3/2}$ for different heat sink temperatures should give parallel straight lines with slopes equal to $(e/2k)T_0^{1/2} Ca/2$. Figure 3 shows three data sets from a NTD Ge sample at different temperatures. Least-square fits to the data over the range $E/T^{3/2} > 400$ V m^{-1} K$^{-3/2}$ show that the slopes are nearly the same. Some of our data from NTD Ge samples show a sharp initial decrease in resistance at very low fields that cannot be fit by the field-effect model (see, for example, the high-temperature curves in Fig. 3). These low-field points were ignored in the fits.

Essentially all of our NTD Ge data and some of our ion-implanted Si data can be fit reasonably well by the exponential field-effect model. However, it does not provide a good
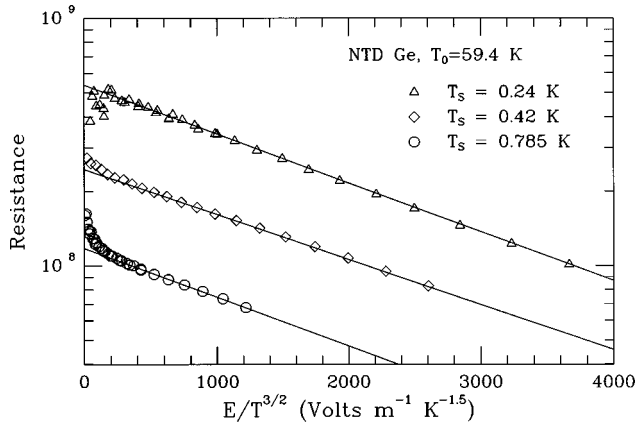
FIG. 3. Resistance vs $E/T^{3/2}$ for a NTD Ge sample with T_0 = 59.4 K at three different heat sink temperatures. According to Eq. (9), the data should follow straight lines with the same slope. The solid lines are fits to the data for $E/T^{3/2}>400$. The slopes agree within their 1σ error bars.

description of the non-Ohmic behavior for much of the Si data. For example, the data in Fig. 4 do not stay on a straight line as would be expected from Eq. (5). The hyperbolic-sine field-effect model can be made to fit in the low-field region, as shown by the solid line, but this model predicts too large an effect at higher field strengths. In addition, ''sinh'' model fits do not result in the monotonic temperature dependence for λ expected from Eq. (9). The empirical ''hot-electron'' model described by Eqs. (6) and (8), however, gives an excellent fit to the data over the entire range of power, as shown by the dashed line. In fitting this model, we obtain T_0 from the measured resistance using low-field data fit to Eq. (2); the ''electron temperature'' T_e can then be obtained from Eq. (6).

Since this hot-electron model makes a definite prediction of the behavior of a given sample as both the power level and the heat sink temperature are varied, we investigated the possibility of using a single set of parameters for all the data from this sample. The apparent electron-lattice thermal con-
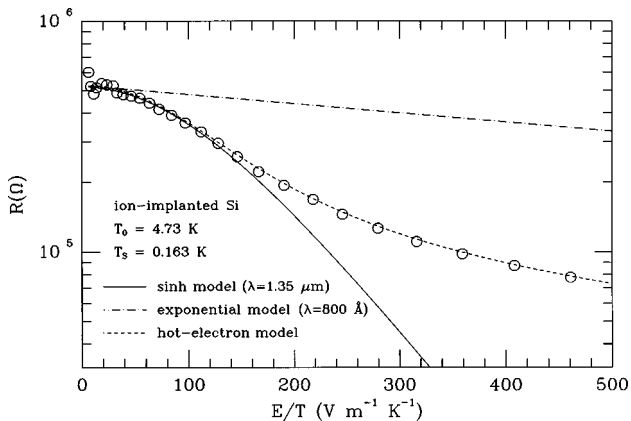

FIG. 4. Resistance vs E/T for an implanted silicon sample. The solid line is the ''sinh'' model, with the hopping length λ adjusted to fit the data in the low-E region. The dashed line is a hot-electron model fit, and the dash-dot line shows the exponential field-effect model, using a value for λ extrapolated from the region where it fits well using $\lambda \propto (Ca/2)(T_0/T)^{1/2}$.
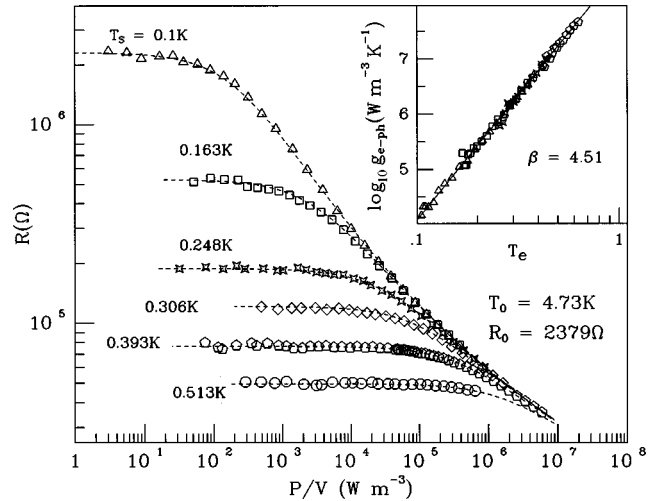

FIG. 5. The data from one ion-implanted silicon sample plotted as R vs P/V for various lattice temperatures. The dashed lines are from the hot-electron model fit. The volume of this sample is 3.0×10^{-14} m^3. The inset shows the derived effective electron-lattice thermal conductivity, $g_{e\text{-ph}}$ [$=d(P/V)/dT$], vs the ''electron temperature'' T_e in log-log scale. Different symbols represent the data taken at different heat sink temperatures T_s and are the same as those used in the main figure.

ductivity, $g_{e\text{-ph}} \equiv d(P/V)/dT$, was determined by observing the rate of change of T_e with applied power. The inset in Fig. 5 shows the resulting values of $g_{e\text{-ph}}$ plotted as a function of T_e. Data taken at different heat sink temperatures are represented by different symbols. The data are all entirely consistent with a single straight line, which gives both the power-law index β and scale factor g_0. For a direct comparison of the model with the data, we replot the data in resistance as a function of the power per unit volume in Fig. 5, along with the model predictions from Eqs. (6) and (8) using β and g_0 from the inset. The hot-electron model, with only two free parameters, matches the data well over the entire range of heat sink temperature and applied power.

The hot-electron model provides a good fit to much but not all of the data from our ion-implanted Si. Figure 6 shows R as a function of P/V for samples with different T_0's. The model fits low-T_0 samples well [Fig. 6(a)], but for higher T_0 [Fig. 6(b)] it underpredicts the non-Ohmic effects at low power levels, particularly at lower heat sink temperatures. For the sample with an even higher T_0 [Fig. 6(c)], the model does not fit the data at any heat sink temperature until very high power levels are reached, although again the deviations are the largest at low temperatures.

To summarize the results of the fits to these two models, we have plotted the quality of the fits on diagrams of T_s versus T_0. Each point in the diagram represents a comparison between the model and a set of data for a sample with characteristic temperature T_0 taken at a heat sink temperature T_s. Results for the exponential field-effect model are shown in Fig. 7. This model fits well for samples with relatively high T_0's taken at low temperatures. For reasons discussed in the next section, all of our data from NTD Ge samples, but only a few sets of data from silicon samples, are in this region.

Figure 8 summarizes the status of the hot-electron model fits on a similar diagram. Fits that are reasonably good ex-
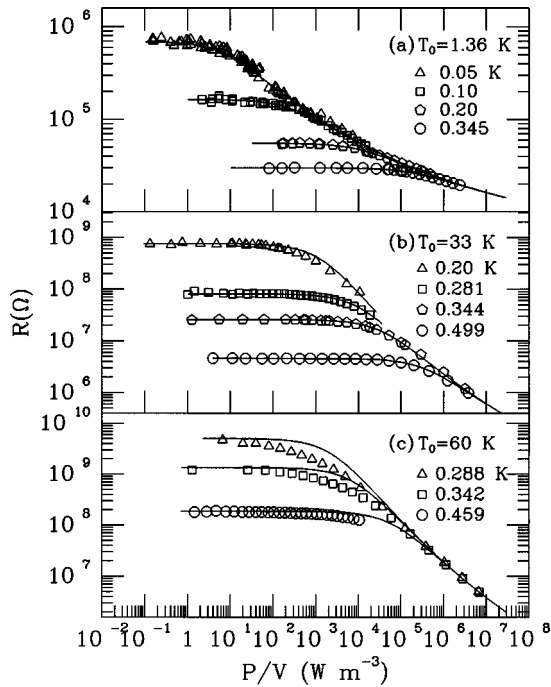
FIG. 6. A comparison of the hot-electron model fits for ion-implanted Si samples with different doping densities. The model fits best for the lowest T_0 (a). Figure (b) shows that for higher T_0 samples, the model starts to fail at low T. For the data in (c) from a sample with even higher T_0, the model fits the data only at very high power densities.

cept at low power levels are labeled ''medium,'' while if the fit is still poor when the resistance drops below 50% of its low-power value, it is labeled ''bad.'' The hot-electron model fits best in the low-T_0–high-T_s region.
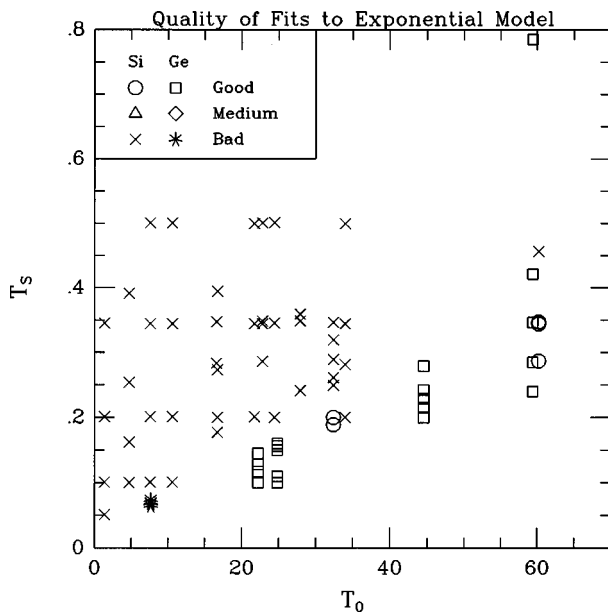

FIG. 7. A summary of the quality of the fits by the exponential field-effect model on a T_s-T_0 diagram. Each point represents a fit to a data set taken at a heat sink temperature T_s for a sample with doping density given by T_0. All of our NTD Ge data are fit well by this model. The data of Wang *et al.* (Ref. 19) for NTD Ge are also shown in this figure as the closely spaced asterisks near the lower left.
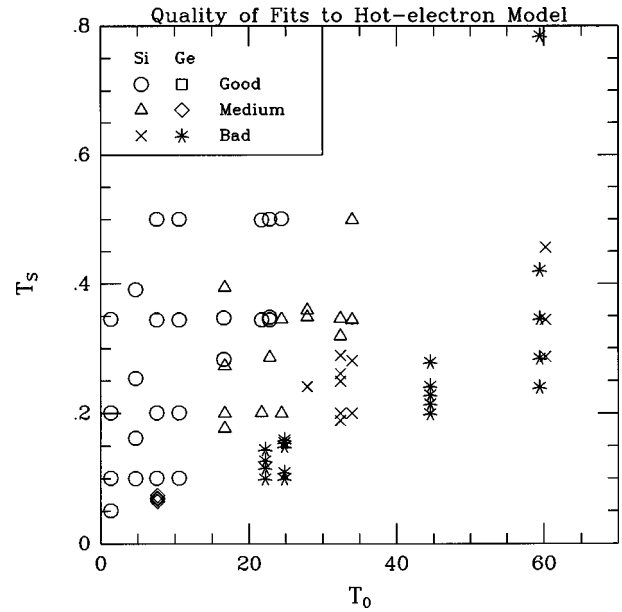

FIG. 8. As in Fig. 7, but for fits to the hot-electron model. The circles and squares mark good fits; triangles and diamonds indicate that the model deviates from the data at low power levels; and crosses and stars mean that the model does not fit until the resistance drops below 50% of its zero-power limiting value. The closely spaced diamonds at the lower left are from the data of Wang *et al.* (Ref. 19).

The results shown in Figs. 7 and 8 suggest that the exponential field-effect model and the hot-electron model fit our data in disjoint regions of the T_s-T_0 diagram. Figure 7 shows that the exponential field-effect model provides good fits to the data in the high-T_0– low-T_s region, while Fig. 8 shows that the hot-electron model fits low T_0 samples at high T_s. In both cases the dividing line between good and poor fits can be described roughly by $T_0/T_s \approx 135$.

Unfortunately, most of our Si measurements lie above this line, and all of our Ge data fall below it. The limit on the range of our Si data is due mainly to the large length to cross-section ratio of even the widest implanted samples, which results in resistances in the $>10^9 \ \Omega$ range in the region of overlap with our Ge samples. On the other hand, the volumes of the NTD Ge samples are ~ 100 times larger than the doped volume of our ion-implanted Si. At the high-power densities where nonlinearities would be measurable in the low-T_0/T_s region, the total power is so large that it is difficult to avoid lattice heating. The few Si samples in the region of good fits of Ge data to the field-effect model also fit this model well, however, and fits to both models become poorer as the boundary is approached. Wang *et al.*[19] have published data from an NTD Ge sample that falls just above the line, and they get reasonably good fits to the hot-electron model. We therefore tentatively conclude that Si and Ge show very similar non-Ohmic behavior, and that its functional form is determined largely by T_0/T_s.

V. DISCUSSION

In this section, we first examine the systematic behavior of the model parameters in the regions of good fits, and then compare our results to other published data.

TABLE I. Parameters from the exponential field-effect model fit.

	T_0 (K)	$Ca/2$ (Å)	a (Å)[a]	C
Ge	24.8	104.5	190	1.10
Ge	25.1	71.2	190	0.74
Ge	44.6	69.5	150	0.92
Ge	59.4	50.6	135	0.74
Si	32.4	47.0		
Si	60.2	32.5		

[a]From magnetoresistance measurements by Ionov, Shlimak, and Matveev (Ref. 28).

We have derived values of $Ca/2$ from the exponential field-effect model [Eq. (10)] fits to our data. The results are shown in Table I. The localization radius a has been determined by Ionov, Shlimak, and Matveev[28] from magnetoresistance measurements for doped Ge samples with doping densities and compensation similar to ours. Theoretical estimates of C range from 0.17 (Ref. 8) to 0.75 (Ref. 7). As shown in Table I, our values of $Ca/2$ are consistent with the measurements of a by Ionov, Shlimak, and Matveev for values of C at the upper end of this range.

The results of our hot-electron model fitting suggest that the free parameters g_0 and β depend only on T_0. Figure 9(a) shows the best-fit values of β as a function of T_0, while Fig. 9(b) shows the derived electron-lattice thermal conductance at 0.1 K (our nominal calorimeter operating temperature) as a function of T_0. We fit straight lines to these plots to obtain empirical expressions for the parameters as functions of T_0:

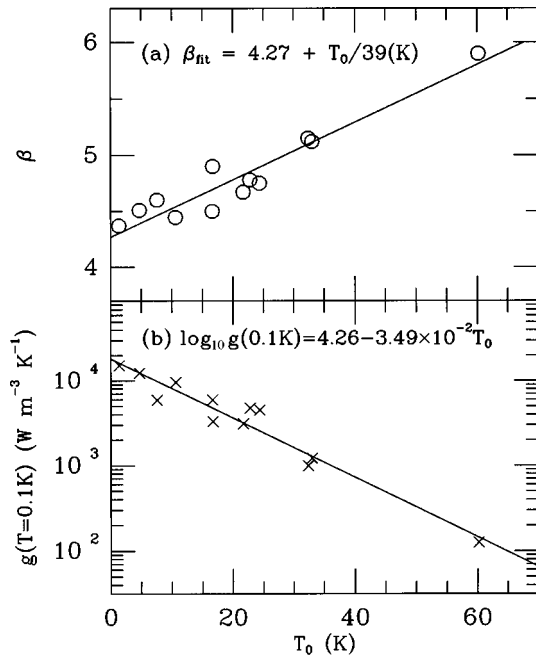$$\beta = 4.27 + \frac{T_0}{39 \ (\mathrm{K})}, \qquad (11)$$

FIG. 9. A summary of the hot-electron model fits to ion-implanted silicon data: (a) the derived power-law index β vs T_0. (b) The effective electron-lattice thermal conductance per unit volume at 0.1 K as function of T_0. The straight lines are least-square fits.
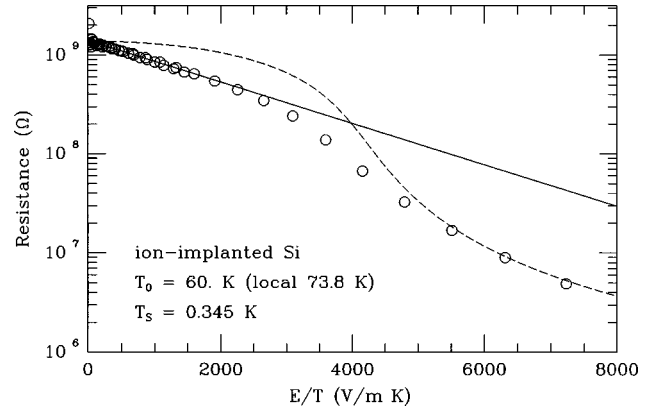

FIG. 10. Data from an ion-implanted Si sample near the T_s-T_0 border line that separates good fits to the two models. The solid line is the fit for the exponential field-effect model, while the dashed line is for the hot-electron model.

$$\log_{10} g(0.1 \ \mathrm{K}) = 4.26 - 3.49 \times 10^{-2} T_0 \ (\mathrm{W \ m^{-3} \ K^{-1}}).$$
$$(12)$$

We know of no well-developed theory for a hot-electron effect in hopping conductivity, but the ability of this simple functional form to give excellent fits to the data over a wide range of temperature and power, and the smooth variation of the parameters with doping density, argue that there is some physical reality in this picture.

As noted in the previous section, the good fits to one or the other of these alternative physical descriptions of nonlinearity are rather cleanly divided by the location of the measurement in T_s (lattice temperature) versus T_0 (doping density) space. This suggests the possibility that these two models describe two real and independent physical effects, which dominate under different conditions of temperature and doping density. The behavior of some samples near the boundary region supports this idea, as shown in Fig. 10. The dashed line is not fit to the data, but is the prediction of the hot-electron model for this T_0 using Eqs. (11) and (12). The solid line is a fit of the exponential field-effect model to only the low-field points. We cannot predict the correlation lengths for silicon, but the derived value of $Ca/2$ is at least reasonable (see Table I). It is clear from the figure that the nonlinearity of this device over the entire range of electric fields could reasonably be described by the sum of these effects. Data from other samples provide counter examples, where the predictions from an extrapolation of one model predict somewhat *more* than the observed nonlinearity. However, the quality of the data and model extrapolations in these cases is not good enough that we would consider the possibility ruled out.

Most published data on non-Ohmic behavior in doped semiconductors have been taken at temperatures above 1 K, or from samples with very low compensation levels.[11–17] We know of only three reports on non-Ohmic effects in hopping conduction below 1.0 K for doped semiconductors with significant compensation.[18–20] All of these are for NTD Ge. One study is reported by Grannan *et al.*[18] for samples with T_0's of 42.4 and 52.5 K. Their measurements cover a temperature range of 0.3–0.8 K but only for very low fields—below the limit for precise measurements with our apparatus. They get good fits to the field-effect model of Eq. (5), but the hopping

scale λ does not show a simple dependence on temperature. The hopping lengths that they derived in this low-field region are longer than what we derived from the moderate field region for data from NTD Ge samples. However, we did observe a sharp initial resistance drop at very low fields from our samples with similar T_0 and T_s (see Fig. 3). Fitting this would give a large λ, so their results may be consistent with ours.

Another study below 1 K, reported by Wang *et al.*,[19] measured a NTD Ge sample with $T_0 = 6.8$ K for heat sink temperatures from 18 to 36 mK. The exponential field-effect model did not fit their data, but the hot-electron model did, except at the low-temperature and low-power extremes of their measurements. Their data are shown in Figs. 7 and 8. Their sample was heated significantly above the heat sink temperature, and we have plotted the points at their derived lattice temperatures. We have Si samples with similar T_0, but we do not have any measurements at such low T. Looking at nearby points, however, this sample seems to be close to the transition, and we might expect a good fit to the hot-electron model except perhaps at the lowest powers. The agreement between the extrapolation of the results from our ion-implanted Si and the results from Wang *et al.* supports our conjecture that the non-Ohmic behaviors of doped Ge and Si are similar.

VI. APPLICATION TO CALORIMETERS

A. Thermometer sensitivity requirements

The effects of this non-Ohmic behavior on the performance of microcalorimeters using doped semiconductors as thermometers arise from the reduction in sensitivity produced by the bias power used to read out the resistance. We can make a quantitative assessment of this performance impact using the results of the analysis of Moseley, Mather, and McCammon[1] for microcalorimeters with ideal resistive thermometers. These results were given in Eq. (1), where the quantity $\sqrt{kT^2C}$ is the rms magnitude of the statistical fluctuations in the energy content of the detector, and ξ is a factor of order unity which depends primarily on the logarithmic temperature sensitivity of the thermometer, α, as shown in Fig. 2 of Ref. 1.

The derivation assumes the signal has zero rise time and decays exponentially with the thermal time constant C/G of the detector (usually shortened somewhat by electrothermal feedback from the bias power). This gives the signal approximately the same power spectrum as the statistical fluctuations in the detector energy as shown in Fig. 11. If this were the only noise source, the signal-to-noise ratio would be constant with frequency, and the signal could be measured with arbitrary accuracy by using an arbitrarily wide bandwidth. The Johnson noise of the thermometer resistance also contributes to the noise, however, and the achievable accuracy depends on the initial ratio r of the fluctuation noise to the Johnson noise below the corner frequency determined by the thermal time constant. It can be shown that $r = \alpha\sqrt{t}$, where t is the fractional temperature increase produced by the bias power, and $\alpha \equiv d\log(R)/d\log(T)$ is the thermometer sensitivity. The value of α is limited by the thermometer technology, but t has an optimum: if the bias current (and t) are very small, the transduced signal and fluc-
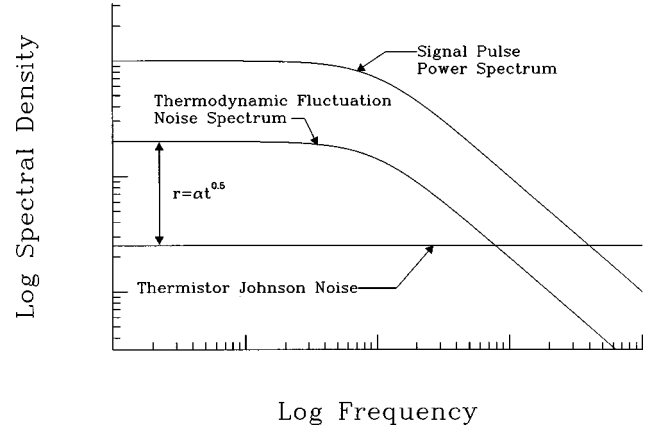

FIG. 11. Diagram showing the signal power spectrum, the thermodynamic fluctuation noise spectrum, and thermometer Johnson noise for an idealized calorimeter. The constant signal to fluctuation-noise ratio would allow arbitrarily good resolution if the usable bandwidth were not limited by the thermometer noise.

tuation noise will be small in comparison to the Johnson noise, while a large readout power will raise the temperature significantly and greatly increase the level of the energy fluctuations. Figure 2 of Ref. 1 also shows the optimum values of t for the case of an ideal thermistor (where α is independent of t), and the resulting values of ξ when the bias power and measurement filter are optimized. For most cases, $t \approx 0.12$ when $\alpha \gg 1$.

When α is small, the thermometer Johnson noise dominates fluctuation noise even at low frequencies, and ξ goes as α^{-1}. For large α, the signal-to-noise ratio below the corner frequency is limited by the fluctuation noise alone, and the thermometer sensitivity determines only the crossover frequency where the fluctuation noise falls below the Johnson noise. This crossover is approximately the usable bandwidth, so in this regime ξ scales as $\alpha^{-1/2}$. The factor ξ and the net energy resolution are independent of the thermal conductance G of the link to the heat sink in this approximation, so one could make the detector as fast or slow as desired for the application without affecting the resolution.

B. Effects of nonlinearity

To see how this is changed by the nonideal behavior of the thermistors, we define an effective α as the logarithmic partial derivative of the resistance with respect to the lattice temperature. Detectors are normally biased at constant current, so we calculate the partial derivative for this condition, but it can easily be calculated for other bias arrangements. For an ideal thermistor, the resistance is a function of the lattice temperature only, so any of these effective α's are equal to the normal α. Figure 12 shows the effective α's calculated from hot-electron model fits to ion-implanted silicon thermistors as a function of the bias power density for two operating temperatures and various doping densities. Quite similar results are obtained from the field-effect model in the parameter range where it also provides a reasonable fit to our data. The figure shows a fairly abrupt drop in sensitivity above some threshold power density. This threshold drops rapidly with decreasing temperature but depends only
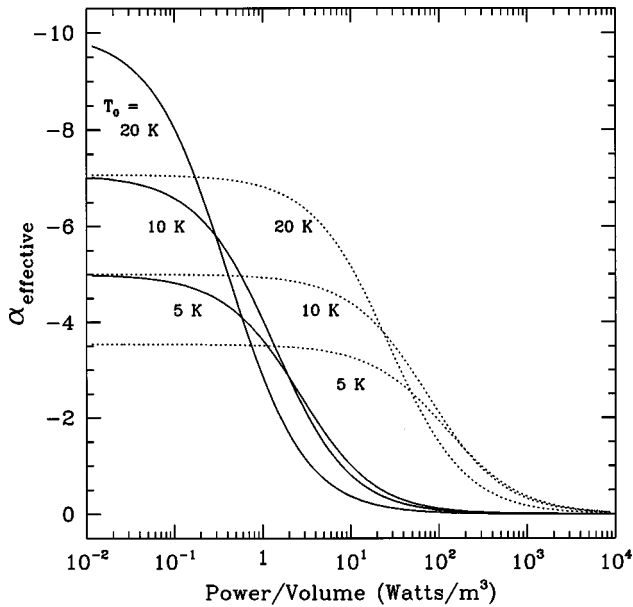
FIG. 12. The predicted logarithmic temperature sensitivity at constant current, $\alpha_{\text{effective}} \equiv (\partial \ln R / \partial \ln T_{\text{lattice}})_{I=\text{const}}$, vs bias power per unit volume (P/V) from the hot-electron model fits shown in Fig. 9. The solid lines are for a lattice temperature $T_s = 0.05$ K, and the dotted lines are for $T_s = 0.1$ K.
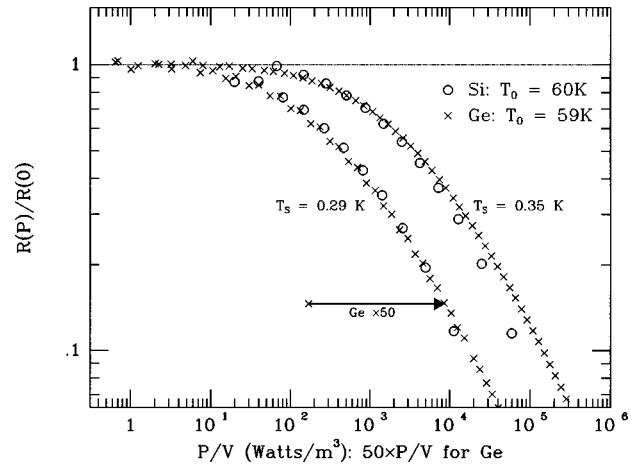

FIG. 13. Resistance as a function of power density at constant lattice temperature for Si and Ge samples with similar temperature sensitivity. The Ge data are plotted at 50 times the actual power density of the measurements.

weakly on doping density, so that devices with different initial sensitivities converge to almost the same sensitivity at moderate power levels.

With these data, it is straightforward to do a numerical optimization of thermistor volume for any given bias power and detector heat capacity. For a fixed coldplate temperature, ΔE is proportional to $\xi C^{1/2}$, where $\xi \propto \alpha^{-1}$ for $|\alpha| < 2$ and $\xi \propto \alpha^{-1/2}$ for $|\alpha| > 4$. The thermistor volume can be increased, reducing P/V and increasing α and the resolution until the thermistor heat capacity starts to contribute significantly to the total C. From the slope of the α versus P/V curves, however, it is clear that if the thermistor heat capacity dominates the total for the detector, the slow improvement in resolution with α for $\alpha \gtrsim 4$ will not make up for the $C^{1/2}$ loss due to the increasing total heat capacity, and the optimum effective α will remain near the 2–4 range.

The ultimate consequence of this limit on P/V is a limit on the *speed* of the detector. The bias optimization requires enough power to raise the absorber temperature by about 12%. This bias power and with it the minimum thermistor volume are therefore proportional to the conductance G of the thermal link. As G is increased to make the detector faster, the thermistor eventually becomes large enough that it dominates the total heat capacity, and from this point the heat capacity rises as fast as the thermal conductance. The thermal time constant $\tau = C/G$ then reaches a minimum limiting value, which for doped silicon thermistors appears to be on the order of 1 ms at 100 mK, and gets longer at lower temperatures. This nonlinearity also becomes a limitation on the ultimate resolution, if there are technological limits on how small G can be made, since the minimum value of $C_{\text{thermistor}}$, and therefore the nominal detector noise, scales with G.

In the context of the hot-electron model for thermistor nonlinearity, there is another mechanism that can limit the

response speed of the detectors. The electrons have an associated heat capacity, and this together with the electron-lattice thermal conductivity should create a time constant that would represent a minimum response time for the detector. The Center for Particle Astrophysics group has observed extra time dependences in their Ge devices that can be fit very well by such a time constant.[19,20] The electronic heat capacities might be expected to vary linearly with temperature, as has been found for the excess heat capacity of doped Si,[29] but the values derived from these fits have temperature dependences that range from much steeper than linear[19] to essentially independent of temperature.[20] In any event, this heat capacity must be part of the total measured heat capacity of the detector, as well as determining the intrinsic time constant of the thermometer. Numerical optimizations we have tried over a wide range of detector parameters show that the electron-lattice thermal conductivity should always be made at least three times larger than the lattice to heat sink thermal conductivity, however, so it appears that for practical detectors, the thermal time constant from the supports will always be considerably longer than the coupling time constant of the electron system.

In a real hot-electron model, one would also expect additional thermodynamic fluctuations in the electron system temperature. These would be particularly deleterious, since they would be transduced at the full thermometer sensitivity, rather than at the smaller effective sensitivity that determines the electrical signal from the lattice fluctuations and the signal. A complete thermistor optimization should include these fluctuations, as well as the loss of temperature sensitivity and the $1/f$ noise discussed in Sec. VI D below.

C. Silicon versus germanium

From the above discussion, it appears that an appropriate ''figure of merit'' for these nonideal thermistors is power handling capability per unit heat capacity (at some reasonable effective α). The power-density part of this can be compared directly for the few cases where we have data from both materials at the same T and T_0. Figure 13 shows the reduction in resistance as a function of power density for

NTD Ge and ion-implanted Si samples with nearly identical T_0's. The Ge data are plotted at 50 times the actual power density, showing that a Si thermistor has about the same nonlinearity as a Ge thermistor with the same sensitivity operated at a 50 times lower power density. The doping density of the Ge is also about 50 times lower than for the Si, so if the curves were plotted in terms of watts per impurity atom instead of watts per m^3, they would lie very closely on top of one another without shifting. If we extrapolate the hot-electron model fits for Si into the region of T_0 and T where we have only Ge data, the comparison favors the germanium more. This may indicate that the relation is complicated, or simply that the empirical model extrapolations are uncertain.

The comparison in terms of heat capacity is more difficult. At temperatures of 100 mK and below, the lattice heat capacity should be negligible compared to that of the impurities. Our measurements of the excess specific heat of the ion-implanted silicon thermistors (after subtracting the heat capacity of the pure silicon) give about $8.5T$ J m^{-3} K^{-2} near 0.1 K, in reasonable agreement with the data of Marko, Harrison, and Quirt.[29] Unfortunately, we know of no similar data for doped germanium. Since the electrical conduction of these samples has the same temperature dependence, however, it is tempting to assume that the energy structure of the states around each cluster of impurities is the same, and that they should have essentially the same heat capacity per impurity site. More work obviously needs to be done in this area, but at this point germanium and silicon appear to have similar figures of merit, and the choice between them can be based on their other attributes: the NTD Ge is easy to make and very predictable, while the ion-implanted Si offers more flexibility in detector construction, particularly for monolithic devices.

D. Excess noise

It is theoretically expected that hopping conduction should show excess noise at some level,[30,31] and we have data over the narrow temperature range 270–350 mK that exhibit $1/f$ noise that scales as the square root of implant volume, as expected for a true bulk effect in the conductor. It gets worse rapidly with decreasing temperature, and is worse at higher T_0's, but is very similar for both NTD Ge and ion-implanted Si.[6,32] We do not yet have much noise data at the lower temperatures of interest, and cannot say whether the excess noise or nonlinearity is the major restriction on how small the thermistors can be made.

E. Other thermometer types

Since the doped semiconductors seem to be intrinsically limited to rather low effective α's are the alternatives more promising? Superconducting transition edge thermometers can have α's exceeding 1000, and despite difficulties with matching to the amplifier noise impedance, promising results have already been obtained.[33] Indeed, the whole idea of using a resistive thermometer to read out a calorimeter seems less than optimum: first, because the power required to read out the resistance heats the detector, and second, because the resistance has Johnson noise. Some work has been done on both inductive and capacitive thermometers.[34,35] A simple analysis shows that these devices can be treated the same as ideal resistive thermometers with an effective α equal to Q times $d\log(Z)/d\log(T)$, where Q^{-1} is the fractional energy loss per cycle and Z is the inductive or capacitive reactance. Since Q's can be on the order of 10^6, these thermometers could theoretically give very large improvements in resolution if suitable amplifiers are available and if the thermometers can be fabricated with sufficiently small heat capacities.

One limitation on this improvement is that having the resolution scale like $\alpha^{1/2}$ depended on the assumption of zero rise time for the signal. The actual rise time includes the event thermalization time, which must be at least a few sound-crossing times in the detector. This finite rise time produces another pole in the signal power spectrum, above which the signal will drop toward the thermodynamic noise. The signal-to-noise ratio will deteriorate rapidly above this frequency, no matter how small the thermometer Johnson noise is in comparison. A simple way of summarizing this is that the useful α of the thermometer can be no larger than the ratio of the *thermal* decay time constant to the rise time of the signal pulse. This means that high-α thermometers are most useful for detectors with fairly long thermal time constants. (See Ref. 36 for a discussion of detector operation in this limit with a magnetic thermometer.)

Biasing a high-α detector for negative electrothermal feedback ($R_{\text{LOAD}} \gg R_{\text{DET}}$ for $\alpha < 0$, $R_{\text{LOAD}} \ll R_{\text{DET}}$ for $\alpha > 0$) can make the signal decay time much shorter than the thermal time constant.[1,37,38] Since the feedback does not affect the signal-to-noise ratio at any frequency (in the absence of significant amplifier noise), the time constant ratio requirement still applies to the thermal time constant only, and this allows the signal decay time to be comparable to the thermalization time. In the linear regime, the same effect could be obtained by high-pass filtering the output pulses, but it has been pointed out by Irwin[38] that the negative electrothermal feedback has the additional advantages of stabilizing the detector responsivity, making it more linear, and, since the deposited energy is almost entirely compensated by a reduction in bias power during the pulse instead of being conducted down the thermal link, higher count rates can be tolerated without excessive shifts in the detector temperature and gain. These benefits can be increased for a given thermometer sensitivity by over-biasing the detector and increasing the electrothermal feedback at some cost in resolution due to the increased detector temperature and thermodynamic fluctuation noise, but the very high sensitivities obtainable with superconducting transition edge thermometers ($\alpha \sim 1000$) provide a high level of feedback even when the bias is optimized for the best small-signal resolution.[39]

The price of using a large negative electrothermal feedback is the requirement for a much quieter amplifier, due to the suppressed signal level. The advent of practical dc superconducting quantum interference devices has largely alleviated this difficulty, however, since they provide an extremely low noise level at a reasonable impedance level for transition edge sensors.

VII. CONCLUSIONS

No single model provides a good description of our non-Ohmic data for all devices and operating temperatures. A

field-assisted tunneling model fits the data at low temperatures for devices with high T_0's (lower doping densities), and its length scale parameter λ shows the expected $T^{-1/2}$ temperature dependence. For higher temperatures and lower T_0's, the data can be fit over a wide range of temperature and power density with an empirical ''hot-electron'' model, where the apparent electron-lattice thermal conductivity and the exponent of its assumed power-law temperature variation depend only on the doping density. The data are generally consistent with a picture where these models represent two physically distinct effects, which exist together but which dominate under different conditions of temperature and T_0.

We see little evidence for any intrinsic differences in the non-Ohmic behavior of NTD germanium and ion-implanted silicon, although differences in the sample geometries prevent us from reaching a definitive conclusion. (As noted in paper I, melt-doped samples of both materials usually show erratic behavior that does not fit any simple pattern. This is possibly due to small-scale fluctuations in the effective doping density.) The power densities required for the onset of significant nonlinearities are much higher in silicon than in germanium, but become almost identical when expressed as power per dopant atom instead of per unit volume.

This nonlinear behavior has a large impact on the performance of cryogenic calorimeters employing these devices as thermometers. Although standard fabrication technology is capable of making the thermometers small enough that their heat capacity could always be negligible, non-Ohmic effects would make such a small thermometer entirely insensitive to temperature changes. Calorimeter design therefore must include a tradeoff of thermometer heat capacity for sensitivity, and this introduces fundamental limits to the speed and energy resolution. While we cannot claim to understand the physical processes producing the nonlinearity, the semi-empirical fits presented here are adequate for optimizing thermometer design for cryogenic detectors with a wide range of characteristics.

---

*Present address: Harvard/Smithsonian Center for Astrophysics, 60 Garden St., Cambridge, MA 02138.

†Present address: Center for Space Research, Rm 37-571, Massachusetts Institute of Technology, Cambridge, MA 02139.

[1] S. H. Moseley, J. C. Mather, and D. McCammon, J. Appl. Phys. **56**, 1257 (1984).

[2] R. Clark Jones, J. Opt. Soc. Am. **43**, 1 (1952).

[3] F. J. Low, J. Opt. Soc. Am. **51**, 1300 (1961).

[4] P. M. Downey, A. D. Jeffries, S. S. Meyer, R. Weiss, F. J. Bachner, J. P. Donnelly, W. T. Lindley, R. W. Mountain, and D. J. Silversmith, Appl. Opt. **23**, 910 (1984).

[5] J. Zhang, W. Cui, M. Juda, D. McCammon, R. L. Kelley, S. H. Moseley, C. K. Stahle, and A. E. Szymkowiak, Phys. Rev. B **48**, 2312 (1993) (paper I); **57**, 4958(E) (1998).

[6] D. McCammon, B. Edwards, M. Juda, P. Plucinsky, J. Zhang, R. L. Kelley, S. Holt, G. Madejski, S. H. Moseley, and A. E. Szymkowiak, in *Low Temperature Detectors for Neutrinos and Dark Matter III*, edited by L. Brogiato, D. V. Camin, and E. Fiorini (Edition Frontieres, Git sur Yvette, 1990), p. 213.

[7] R. M. Hill, Philos. Mag. **24**, 1307 (1971).

[8] M. Pollak and I. Reiss, J. Phys. C **9**, 2339 (1976).

[9] N. Apsley and H. P. Hughes, Philos. Mag. **30**, 963 (1974).

[10] B. I. Shklovskii, Fiz. Tekh. Poluprovodn. **10**, 1440 (1976) [Sov. Phys. Semicond. **10**, 855 (1976)].

[11] D. Redfield, Adv. Phys. **24**, 463 (1975).

[12] A. G. Zabrodskii and I. S. Shlimak, Fiz. Tekh. Poluprovodn. **11**, 736 (1977) [Sov. Phys. Semicond. **11**, 430 (1977)].

[13] T. F. Rosenbaum, K. Andres, and G. A. Thomas, Solid State Commun. **35**, 663 (1980).

[14] A. N. Ionov, M. N. Matveev, I. S. Shlimak, and R. Rentch, Pis'ma Zh. Eksp. Teor. Fiz. **45**, 248 (1987) [JETP Lett. **45**, 310 (1987)].

[15] Chen Gang, H. D. Koppen, R. W. van der Heijden, A. T. A. M. de Waele, H. M. Gijsman, and F. P. B. Tielen, Solid State Commun. **72**, 173 (1989).

[16] T. W. Kenny, P. L. Richards, I. S. Park, E. E. Haller, and J. W. Beeman, Phys. Rev. B **39**, 8476 (1989).

[17] I. N. Timchenko, V. A. Kasiyan, D. D. Nedeoglo, and A. V. Simashkevich, Fiz. Tekh. Poluprovodn. **23** 240 (1989) [Sov. Phys. Semicond. **23**, 148 (1989)].

[18] S. M. Grannan, A. E. Lange, E. E. Haller, and J. W. Beeman, Phys. Rev. B **45**, 4516 (1992).

[19] Ning Wang, F. C. Wellstood, B. Sadoulet, E. E. Haller, and J. Beeman, Phys. Rev. B **41**, 3761 (1990).

[20] E. Aubourg, A. Cummings, T. Shutt, W. Stockwell, P. D. Barnes, Jr., A. DaSilva, J. Emes, E. E. Haller, A. E. Lange, R. R. Ross, B. Sadoulet, G. Smith, N. Wang, S. White, B. A. Young, and D. Yvon, J. Low Temp. Phys. **93**, 289 (1993).

[21] W. A. Little, Can. J. Phys. **37**, 334 (1959).

[22] V. A. Shklovskij, J. Low Temp. Phys. **41**, 375 (1980).

[23] A. C. Anderson and R. E. Peterson, Phys. Lett. **38A**, 519 (1972).

[24] P. W. Anderson, E. Abrahams, and T. V. Ramakrishnan, Phys. Rev. Lett. **43**, 718 (1979).

[25] M. L. Roukes, M. R. Freeman, R. S. Germain, R. C. Richardson, and M. B. Ketchen, Phys. Rev. Lett. **55**, 422 (1985).

[26] N. Perrin, J. Low Temp. Phys. **93**, 313 (1993).

[27] E. E. Haller, IR Phys. **25**, 257 (1985).

[28] A. N. Ionov, I. S. Shlimak, and M. N. Matveev, Solid State Commun. **47**, 763 (1983).

[29] J. R. Marko, J. P. Harrison, and J. D. Quirt, Phys. Rev. B **10**, 2448 (1974).

[30] B. I. Shklovskii, Solid State Commun. **33**, 273 (1980).

[31] Sh. M. Kogan and B. I. Shklovskii, Fiz. Tekh. Poluprovodn. **15**, 1049 (1981) [Sov. Phys. Semicond. **15**, 605 (1981)].

[32] D. McCammon, W. Cui, M. Juda, J. Morgenthaler, J. Zhang, R. L. Kelley, S. S. Holt, G. M. Madejski, S. H. Moseley, and A. E. Szymkowiak, Nucl. Instrum. Methods Phys. Res. A **326**, 157 (1993).

[33] P. Colling, A. Nucciotti, C. Bucci, S. Cooper, P. Ferger, M. Frank, U. Nagel, F. Proebst, and W. Seidel, Nucl. Instrum. Methods Phys. Res. A **354**, 408 (1995).

[34] D. G. McDonald, Appl. Phys. Lett. **50**, 775 (1987).

[35] E. H. Silver *et al.*, Nucl. Instrum. Methods Phys. Res. A **277**, 657 (1989).

[36] M. Büxhler, E. Umlauf, and J. C. Mather, Nucl. Instrum. Methods Phys. Res. A **346**, 225 (1994).

[37] J. C. Mather, Appl. Opt. **21**, 1125 (1982).

[38] K. D. Irwin, Appl. Phys. Lett. **66**, 1998 (1995).

[39] J. C. Mather, Appl. Opt. **23**, 584 (1984).